Appl. Phys. A 76, 339–350 (2003)
DOI: 10.1007/s00339-002-1818-5

Applied Physics A
Materials Science & Processing

L.V. ZHIGILEI

Dynamics of the plume formation and parameters of the ejected clusters in short-pulse laser ablation

Department of Materials Science & Engineering, University of Virginia, 116 Engineer's Way, Charlottesville, Virginia 22904, USA

Received: 13 October 2001/Accepted: 18 July 2002
Published online: 25 October 2002 •

ABSTRACT The dynamics of the early stages of the ablation plume formation and the mechanisms of cluster ejection are investigated in large-scale molecular dynamics simulations. The cluster composition of the ablation plume has a strong dependence on the irradiation conditions and is defined by the interplay of a number of processes during the ablation plume evolution. At sufficiently high laser fluences, the phase explosion of the overheated material leads to the formation of a foamy transient structure of interconnected liquid regions that subsequently decomposes into a mixture of liquid droplets, gas-phase molecules, and small clusters. The ejection of the largest droplets is attributed to the hydrodynamic motion in the vicinity of the melted surface, especially active in the regime of stress confinement. Spatially resolved analysis of the dynamics of the plume formation reveals the effect of segregation of the clusters of different sizes in the expanding plume. A relatively low density of small/medium clusters is observed in the region adjacent to the surface, where large clusters are being formed. Medium-size clusters dominate in the middle of the plume and only small clusters and monomers are observed near the front of the expanding plume. Despite being ejected from deeper under the surface, the larger clusters in the plume have substantially higher internal temperatures as compared to the smaller clusters. The cluster-size distributions can be relatively well described by a power law $Y(N) \sim N^{-\tau}$ with exponents different for small, up to ~ 15 molecules, and large clusters. The decay is much slower in the high-mass region of the distribution.

PACS 79.20.Ds; 61.80.Az; 02.70.Ns

1 Introduction

Laser ablation is a phenomenon used in a number of important practical applications, such as surface microfabrication and processing [1], pulsed laser deposition (PLD) of films and coatings [2], laser surgery [3], and matrix-assisted laser desorption/ionization (MALDI) of biomolecules for mass-spectrometric investigations [4, 5]. In many of these applications the ability to predict and control the cluster composition of the ablation plume is critical. In particular, the presence of clusters or particulates in the ablation plume can have an adverse effect on the quality of homogeneous thin films grown in PLD [2], whereas formation of debris and redeposition of ejected particulates can cause problems in manufacturing of surface microstructures. On the other hand, generation of clusters in laser ablation can be turned to useful account in production of nano- and micrometer-sized particles, ultra-fine powders, nanocomposites, and thick coatings [6–8]. A possible important role of the ejection of molecular clusters in ionization in MALDI has been recently discussed and supported by experimental observations [9–12].

The implications of cluster ejection for practical applications have motivated a number of experimental and theoretical investigations aimed specifically at understanding the conditions and mechanisms of cluster production in laser ablation [6, 13–19]. For organic targets, cluster-size distributions have been studied in trapping plate experiments performed by Handschuh et al. [13] for ultra-violet (UV)-MALDI conditions, laser-induced thermal desorption, and infra-red (IR) polymer ablation. The results show that both the fraction of the ejected clusters in the plume and the characteristic sizes of the clusters have a strong dependence on the type of the laser desorption/ablation technique used and the laser fluence. The ejection of charged clusters of different sizes, from submicron to 10 μm, has been observed by Heitz and Dickinson [6] in laser ablation of hot-pressed polymeric powders. The observed particles have been separated into several distinct classes based on the particle morphologies, composition, and electrostatic charge. Indirect evidence of the ejection of molecular clusters in MALDI has been obtained in post-ionization time-of-flight mass spectrometry experiments by Hankin and John [20]. Recent observations by Fournier et al. of a non-linear dependence of the time of flight on the delay time in the delayed extraction experiments has been explained by a delayed ion formation from higher-mass precursors [12]. In laser ablation of inorganic materials, the ejection of liquid and/or solid particulates has been observed for metals [21–23] semiconductors [24–26], and dielectrics [15]. In general, cluster production in laser ablation has been observed for a wide range of target materials and appears to be a rather general phenomenon.

A number of scenarios of cluster formation in laser ablation have been discussed in the literature.

✉ Fax: +1-434/982-5660, E-mail: lz2n@virginia.edu

1.1 *Condensation in the expanding plume*

In many cases observation of small clusters is attributed to the collision-induced condensation in the dense regions of the ejected plume [14, 17–19]. An efficient cluster formation can be expected when the ambient gas pressure is sufficiently high so that many collisions of vapor species can occur between target and collector, although condensation can take place under vacuum conditions as well [14]. Normally, condensation is used to explain observation of small clusters composed of tens to thousands of atoms/molecules. Formation of larger sub-micron and micron-sized particles would require an unrealistically high number of collisions to occur in the expanding plume. Therefore, direct ejection of clusters from the target is likely to be responsible for the formation of larger clusters.

1.2 *Phase explosion*

Explosive boiling or phase explosion has been discussed as a primary mechanism of short-pulse laser ablation in a number of works [21, 24, 27–32]. Theoretically, this mechanism and its relevance to the conditions realized in pulsed laser ablation have been analyzed based on classical thermodynamics [27, 29, 30]. The surface region, overheated up to the limit of its thermodynamic stability by short-pulse laser irradiation, is predicted to undergo a rapid transition from an overheated liquid to a mixture of vapor and liquid droplets. Experimental observations of the existence of a well-defined threshold fluence for the onset of the droplet ejection, as well as a steep increase of the ablation rate at the threshold, have been interpreted as evidence of the transition from normal vaporization to phase explosion [21, 24, 25, 30].

1.3 *Hydrodynamic sputtering*

The term hydrodynamic sputtering is typically used to refer to a range of processes in which large droplets are ejected as a result of a transient melting and motion of a liquid caused by steep thermal gradients and relaxation of the laser-induced pressure [15, 16, 22, 33]. Formation of hydrodynamic instabilities in a single-shot ablation [16, 23] as well as the appearance, gradual growth, and eventual separation of molten asperities due to the combined action of inertial and surface tension forces in a multi-pulse irradiation regime [16, 22, 33] have been discussed. Analysis of surface morphology of irradiated targets provides strong support for the hydrodynamic mechanism of large-droplet ejection in metals [16, 22, 23].

1.4 *Photomechanical effects: exfoliation and spallation*

The ejection of large liquid droplets and/or solid particulates can also be caused by photomechanical effects driven by the relaxation of the laser-induced stresses [6, 14, 15, 25, 26, 32, 34, 37, 38]. The magnitude of the laser-induced stresses and the role of the associated photomechanical effects in the material ejection become significant under conditions of stress confinement, when the laser pulse duration is shorter then the time needed for mechanical equilibration of the absorbing volume [32, 34, 35, 37–41]. In the regime of stress confinement the laser-induced stresses can exceed the dynamic tensile strength of the target material, causing cavitation and disruption of a liquid surface region or mechanical fracture/spallation of a solid target. The ejection of large droplets or fractured solid fragments has been observed in the regime of stress confinement both experimentally [15, 34, 35, 40] and in simulations [32, 37, 38]. One can expect that microstructure, surface roughness, and mechanical properties of the target material play an important role in disintegration of the target in this regime.

While the observation of small clusters, droplets, and large particulates in laser ablation is consistent and a number of mechanisms of cluster formation have been discussed, a clear picture of the interplay of different processes occurring during the ablation plume evolution and their relation to the parameters of the observed clusters is still lacking. In this paper the mechanisms of cluster formation are investigated in a series of large-scale molecular dynamics (MD) simulations of laser ablation performed for a model molecular solid. A comprehensive molecular-level picture of the early stages of the ablation plume development emerges from the simulations. The abundance of clusters, their velocities, and their internal temperatures are studied for a range of the irradiation parameters and related to the physical processes leading to the material ejection.

2 Computational model

The main challenge in application of the MD method to the analysis of laser ablation is that the material ejection involves a collective motion of a large number of atoms or molecules in the surface region of the irradiated target. The systems that have to be simulated in order to reproduce the collective processes in laser ablation of a molecular solid are too large to be modeled by a conventional atomic level MD method. A breathing sphere model developed recently for MD simulations of laser ablation of organic solids has significantly expanded the time and length scales accessible for the simulations [42]. The model has been extensively used in simulations of laser ablation of organic materials and has yielded a wealth of information on the ablation mechanisms [31, 32, 36, 42], parameters of the ejected plume (velocity distributions of matrix and analyte molecules in MALDI [43, 44] and cluster ejection [31, 32, 36, 38]) and their dependence on the irradiation conditions (laser fluence [31, 32, 36, 37, 42], pulse duration [32, 37], and initial temperature of the sample [37]).

The breathing sphere model is described in detail in [42]. Briefly, the model assumes that each molecule (or an appropriate group of atoms) can be represented by a single particle that has the true translational degrees of freedom but an approximate representation of internal degrees of freedom. The parameters of the interparticle interaction are chosen to reproduce the van der Waals interaction in a molecular solid with the cohesive energy of 0.6 eV, an elastic bulk modulus of ~ 5 GPa, and a density of 1.2 g/cm^3. A mass of 100 Da is attributed to each molecule. In order to simulate molecular excitation by photon absorption and vibrational relaxation of the excited molecules, an additional internal degree of freedom is attributed to each molecule. This internal degree of freedom, or breathing mode, is realized by allowing the particles to

change their sizes. The parameters of a potential function ascribed to the internal motion control the rate of the conversion of internal energy of the molecules excited by the laser to the translational and internal motion of the other molecules. Since the molecules rather than the atoms are the particles of interest in the model, the system size can be large enough to model the collective dynamics leading to laser ablation and damage. Moreover, since explicit atomic vibrations are not followed, the time step in the numerical integration of the equations of motion can be much longer and the dynamics in the irradiated sample can be followed for as long as nanoseconds.

In the present study the breathing sphere model is applied to study the dynamics of the cluster formation during the initial stage of the ablation plume development. In order to minimize the effect of the finite size of the simulated system on cluster ejection and to obtain sufficient data for the analysis of cluster-size distributions, a significantly larger, as compared to the simulations reported before [31, 32, 36–38, 42–44], computational cell with dimensions of $40 \times 40 \times 90\ \mathrm{nm}^3$ (1 015 072 molecules) is used in the simulations. Periodic boundary conditions imposed in the directions parallel to the surface simulate the situation in which the laser spot diameter is much large compared to the laser penetration depth so that the effects of the edges of the laser beam can be neglected. At the bottom of the MD computational cell we apply the dynamic boundary condition developed to avoid artifacts due to reflection of the laser-induced pressure wave from the boundary of the computational cell. The boundary condition accounts for the laser-induced pressure-wave propagation as well as the direct laser energy deposition in the boundary region, as described in [45].

The laser irradiation is simulated by vibrational excitation of molecules that are randomly chosen during the laser pulse duration. The probability of a molecule to be excited is modulated by Lambert–Beer's law to reproduce the exponential attenuation of the laser light with depth, with an absorption depth of 50 nm. The vibrational excitation is modeled by depositing a quantum of energy equal to the photon energy into the kinetic energy of internal motion of a given molecule. Irradiation at a wavelength of 337 nm (3.68 eV) is simulated in this study. The total number of photons entering the model during the laser pulse is determined by the laser fluence. The values of the laser pulse duration, $\tau_p = 15$ ps and $\tau_p = 150$ ps, are chosen in order to investigate cluster ejection in two distinct irradiation regimes: stress confinement and thermal confinement [32]. The pulse duration of 150 ps is short relative to the characteristic thermal diffusion time across the absorption depth, $\tau_{th} \sim 10$ ns, but longer than the time of mechanical equilibration of the absorbing volume, $\tau_s \sim 20$ ps. Thus, the simulations with 150-ps pulses are performed in the regime of thermal confinement but not thermoelastic stress confinement. For the 15-ps laser pulse the condition for stress confinement, $\tau_p \leq \tau_s$, is satisfied. In this case a high thermoelastic pressure can be expected to result from the fast energy deposition in the absorption region leading to an increasing role of photomechanical effects in material ejection.

Although the results presented in this paper are obtained for a model molecular system, the revealed physical mechanisms leading to the material ejection and cluster formation can be relevant to other materials as well. Primary mechanisms of laser excitation of optically active states in a solid, as well as characteristic times and channels of the relaxation/thermalization of the absorbed laser energy, can be drastically different for different types of material. Thus, system-specific computational approaches should be developed for incorporation of the description of the interaction of laser light with the target material into the classical MD technique. Examples of the computational approaches are the breathing sphere model described above for molecular systems, the two-temperature model for the description of the laser light absorption by the conduction-band electrons and energy exchange between the electrons and the phonons in metals [46–49], as well as a description of the relaxation of a dense gas of hot electrons and holes generated by the laser pulse in semiconductors [50]. After thermalization of the deposited laser energy, though, the response of different materials to the fast laser heating may include similar processes such as melting and hydrodynamic motion of the liquid layer, explosive boiling, or photomechanical spallation [27–41, 46–50]. Therefore, the computational results presented in this paper for laser ablation of a molecular target may provide some insights into the mechanisms of laser ablation of other materials as well.

3 Results and discussion

The results of large-scale molecular dynamics simulations are used in this work to perform a detailed analysis of the dynamics of the ablation plume formation and the mechanisms of cluster ejection. The abundance of the ejected clusters, their velocities, internal temperatures, and spatial distribution in the ablation plume are studied and related to the physical mechanisms of cluster formation. The effect of the laser fluence and pulse duration on the parameters of the ejected plume are discussed and related to the transition between the thermal and stress confinement irradiation conditions.

3.1 *The dynamics of the ablation plume formation*

In this section the dynamics of disintegration and ejection of a surface region of the irradiated target is analyzed for a simulation performed for a laser pulse duration of 150 ps, a fluence of 61 $\mathrm{J/m^2}$, and a laser penetration depth of 50 nm. The laser fluence used in this simulation is 1.75 times the threshold fluence for the onset of the massive material ejection or ablation [32]. The pulse duration of 150 ps corresponds to the irradiation regime of thermal confinement, as discussed in Sect. 2. This regime is also characteristic for nanosecond laser ablation of strongly absorbing organic materials, e.g. in UV-MALDI [4, 5]. It has been demonstrated that in the regime of thermal confinement the amount of energy deposited by the laser pulse, rather than the pulse duration, determines the desorption/ablation process [51]. The results discussed below could be, therefore, related to a wide range of applications of short-pulse laser ablation in which the condition for the thermal confinement is satisfied. An analysis of the dynamics of the ablation plume formation in the regime of stress confinement is given in [52].

Snapshots from the simulation, Fig. 1, give a visual picture of the active processes occurring in the vicinity of the irradi-

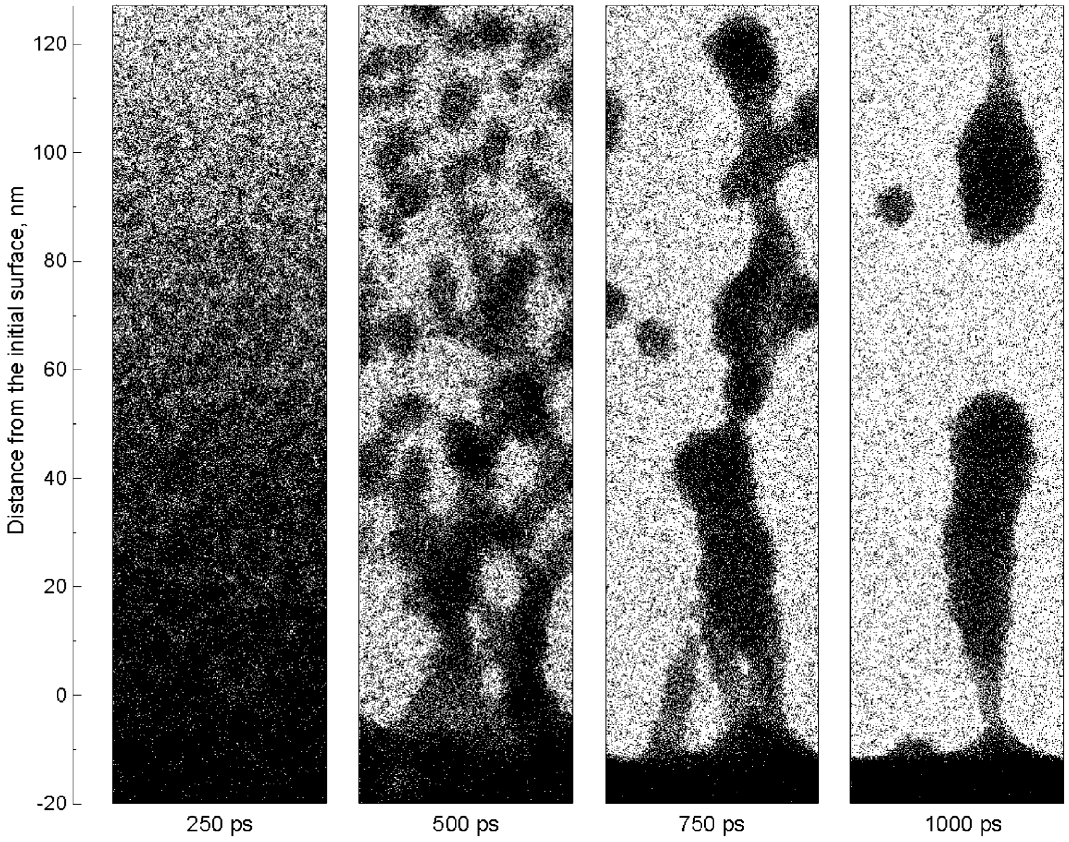

FIGURE 1 Snapshots from the simulation of laser ablation in the regime of thermal confinement. The lase pulse duration is 150 ps and fluence is 61 J/m^2 (1.75 times the ablation threshold fluence)

ated surface during the first nanosecond following the laser irradiation. In the first snapshot, shown for 250 ps, 100 ps after the end of the laser pulse, we see a homogeneous expansion of a significant part of the surface region. The homogeneous expansion is followed by the appearance of density fluctuations and gradual decomposition of the expanding plume into gas-phase molecules and liquid-phase regions. A closer view at a snapshot of a part of the ablation plume taken at a time of 200 ps, when the density fluctuations are apparent, is shown in Fig. 2. Growth of the density fluctuations and the decomposition of the expanding plume lead to the formation of a foamy transient structure of interconnected liquid regions, as shown in the snapshot at 500 ps. The foamy transient structure subsequently decomposes into separate clusters, snapshots at 750 ps and 1000 ps, which gradually develop into well-defined spherical liquid droplets. Figure 1 shows the processes induced by laser irradiation only in a rather narrow area in the vicinity of the original surface of the target. A view for a much broader range of distances from the original surface, up to 0.5 μm, is shown for a time of 650 ps in Fig. 3. From this figure we see that clusters of a wide range of sizes are being formed during the first nanosecond of the ablation plume formation. There is an apparent segregation of clusters of different sizes in the ablation plume: there are virtually no small and medium-size clusters in the region adjacent to the surface, where only large clusters are being formed, medium-size clusters dominate in the middle of the plume, from 120 nm to 220 nm, and small clusters are observed in the top part of the region shown in the figure. The snapshots shown in Figs. 1 and 3 suggest that cluster formation proceeds differently in different parts of the ablation plume and a de-

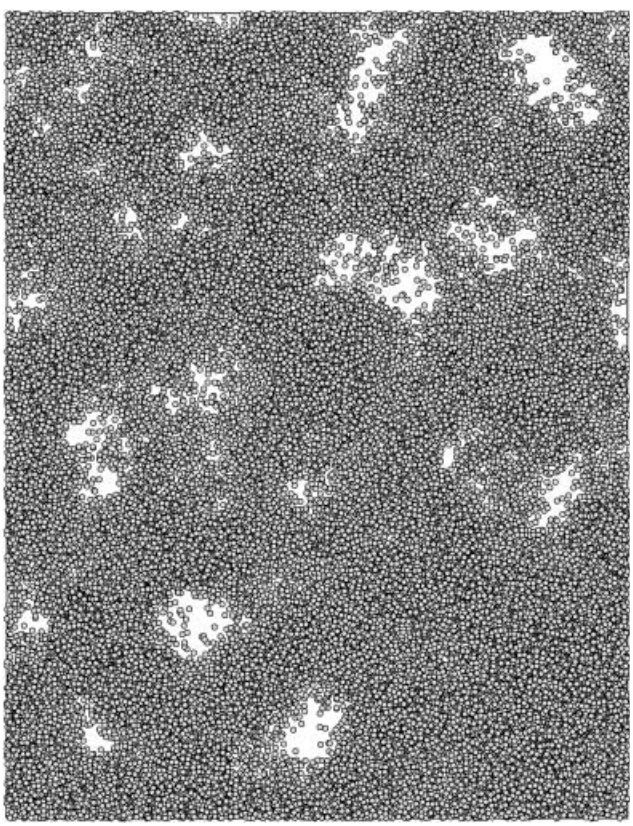

FIGURE 2 A closer look at the foamy transient structure of interconnected liquid clusters and individual molecules formed in the process of explosive homogeneous boiling of overheated material. A slab of dimensions $40 \times 50 \times 10$ nm is cut from the ablation plume obtained in the simulation illustrated in Fig. 1 at a time of 200 ps

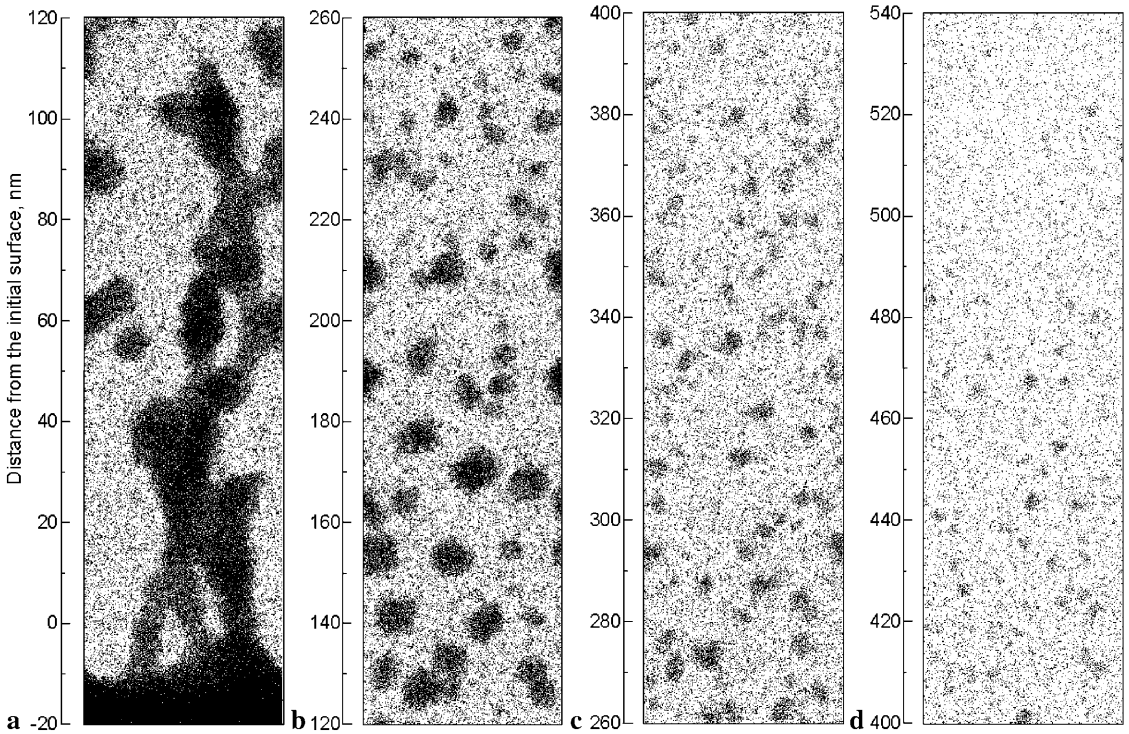

FIGURE 3 Snapshot from the simulation illustrated by Fig. 1 at a time of 650 ps. A broader range of distances from the orininal surface is shown as compared to Fig. 1

tailed spatially resolved analysis of the dynamics of the plume formation is needed in order to obtain complete information on cluster generation.

Figure 4 illustrates schematically a method used in this work to perform a spatially resolved analysis of the dynamics of the ablation plume formation. The computational cell is divided into layers that are parallel to the initial surface and contain the same number of molecules (3 nm of the original solid $\approx$ 34 000 molecules in the $40 \times 40 \times 90$ nm^3 computational cell). Density distributions for each layer are calculated at different times during the simulation. The analysis allows one to study the character of the explosive disintegration of the overheated material [27, 29–32] that originates from different depths under the surface and reaches different maximum temperatures by the end of the laser pulse. The material ejected from the top layers of the irradiated sample is highly overheated and quickly, within first 100 ps, decomposes into very small clusters and gas-phase molecules. There are only small density fluctuations in the topmost layer (top 34 000 molecules in the plume, not shown) and the density distribution remains essentially homogeneous. The homogeneous density distribution indicates that the front of the ablation plume is predominantly composed of the gas-phase molecules. In the second layer, a separation into lower-density and higher-density regions can be observed, Fig. 5. This separation corresponds to the formation of small molecular clusters that can be seen in Fig. 3c. The regions of higher density in Fig. 5 are formed within the first $\sim$ 300 ps and become somewhat more pronounced at later times. The process of the decomposition of the expanding material into the liquid-phase and gas-phase regions observed in the middle of the ejected plume, Fig. 6, is slower and proceeds through the

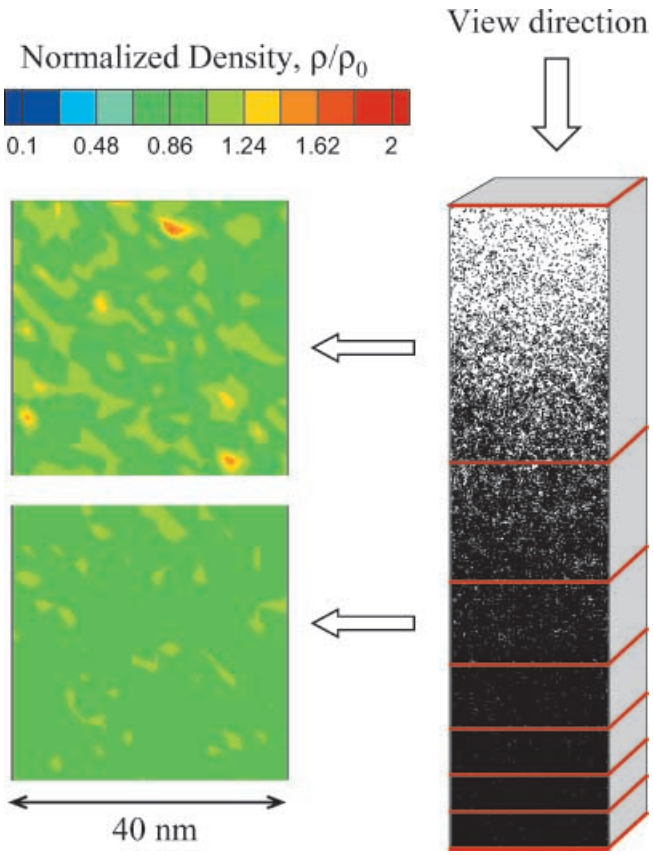

FIGURE 4 Schemtic illustration of the method used to analyze the dynamics of cluster formation in the ablation plume (see Figs. 5 to 7). The computational cell is divided into layers. Each layer contains the same number of molecules ($\sim$ 34 000 molecules – corresponds to 3 nm of the orininal solid.) Density distributions for the same layer are calculated at different times during the simulation

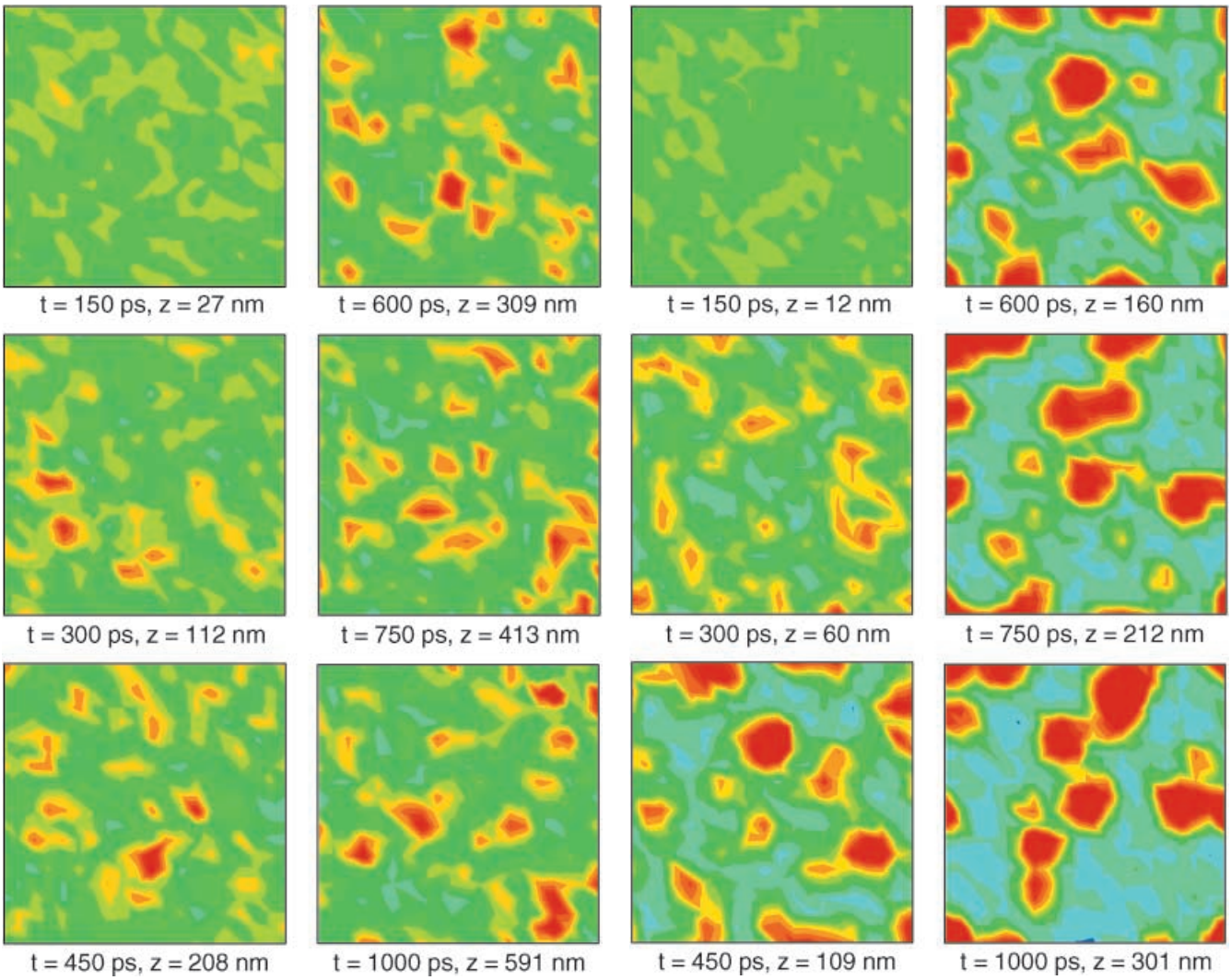

FIGURE 5 Density plots showing the dynamics of cluster formation near the front of the ablation plume (second layer) for the simulation with the laser pulse duration of 150 ps and fluence of 61 J/m^2. Time, t, and layer position relatively to the initial surface of the irradiated target, z, are shown in the figure. Layer position z is the average of the positions of all molecules that belong to the layer. Initial position at $t = 0$ is $z = -4.5$ nm. See Fig. 4 for explanation and scale of the contour plots

FIGURE 6 Density plots showing the dynamics of cluster formation in the middle of the ablation plume (fourth layer). Initial position at $t = 0$ is $z = -10.5$ nm. See Figs. 4 and 5 for explanation and scale of the contour plots

formation of a transient structure of interconnected liquid regions. The liquid regions become more defined with time and, by ~ 500 ps the transient structure disintegrates into separate liquid droplets. Material disintegration in the rear part of the plume proceeds through the similar steps – formation and decomposition of the transient foamy structure of interconnected liquid regions, Fig. 7 The fraction of the liquid phase in this part of the plume is larger and the formation of a few large droplets proceeds through a coarsening of the initial transient foamy structure formed at earlier times of the plume expansion. Coarsening of the liquid regions and formation of large droplets is nearly complete by 1 ns, although relaxation of the shape of the largest droplets takes a somewhat longer time, Fig. 1. The density of the slowly moving droplets in the tail of the plume is sufficiently high and one can expect that collisions between the droplets can lead to their coalescence [53, 54] and formation of even larger droplets.

A further development of cluster composition of the plume due to the cluster–cluster collisions, evaporation, and condensation is slow and cannot be addressed in MD simulations. In order to overcome this limitation, we propose to use a combined multi-scale computational model, in which the direct-simulation Monte Carlo (DSMC) method is used to study the processes occurring during the ablation plume expansion on the time and length scales of a real experimental configuration [52, 55, 56]. In this model, the results obtained by the end of a MD simulation are used as an input for a DSMC simulation of the further plume evolution.

The picture of the explosive ejection and decomposition of the ejected material into individual molecules and liquid droplets is consistent with the explosive vaporization mechanism predicted from classical thermodynamics [27–29]. It has be discussed that short pulse laser irradiation can overheat the absorbing region up to the limit of thermodynamic stability, leading to a rapid phase transition of the overheated material into a mixture of gas-phase molecules and liquid droplets. The relative amount of the gas-phase molecules is related to the de-

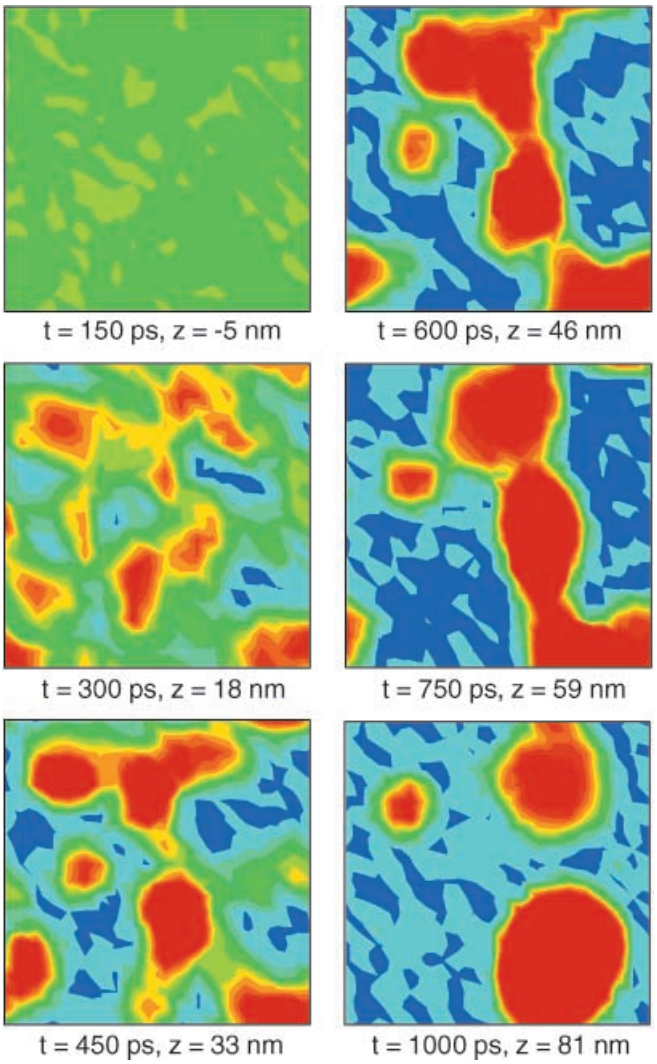

FIGURE 7 Density plots showing the dynamics of cluster formation in the tail of the ablation plume (seventh layer). Initial position at $t = 0$ is $z = -19.5$ nm. See Figs. 4 and 5 for explanation and scale of the contour plots

gree of overheating [27] and provides a driving force for the expansion of the ablation plume. In the simulation discussed above, the degree of the overheating and the fraction of the vaporized material are decreasing with depth under the irradiated surface, resulting in a strong dependence of the character of the material decomposition on the depth of origin of the ejected material.

3.2 *Cluster velocities, internal temperature, and spatial distribution in the plume*

The results of the spatially resolved analysis of the dynamics of the plume formation, Figs. 5–7, suggest that clusters of different sizes tend to be localized in different parts of the ejected plume. Large clusters are formed in the region adjacent to the surface, Fig. 7, medium-size clusters are formed in the middle of the plume, Fig. 6, and small clusters are formed in the top part of the plume, Fig. 5. This observation can be further illustrated by analysis of the spatial distribution of clusters in the plume. In order to obtain a statistically adequate representation of the spatial distribution of large clusters in the ablation plume, the distributions are plotted for groups of clusters. Four distributions, for individual molecules, for medium-size molecular clusters (16 to 100 molecules), as well as for large (101 to 1000 molecules) and very large (more than 1000 molecules) molecular clusters are shown in Fig. 8. The medium-size clusters are localized in the middle of the expanding plume, whereas the larger clusters formed later during the plume development, Fig. 7, tend to be slower and are closer to the original surface.

The velocities of the ejected molecules and clusters can be described by the distribution of their radial (parallel to the surface) velocity components, as well as the flow velocities in the direction normal to the surface for different parts of the plume and for different plume components. The plot of the flow velocity as a function of the distance from the initial surface, Fig. 9, shows that identical linear dependences on the distance from the surface, characteristic of the free-expansion model, apply to all components of the plume. The clusters of different sizes are entrained into the expanding plume and are moving along with the individual molecules with nearly the same velocities. This effect of entrainment of molecular clusters can

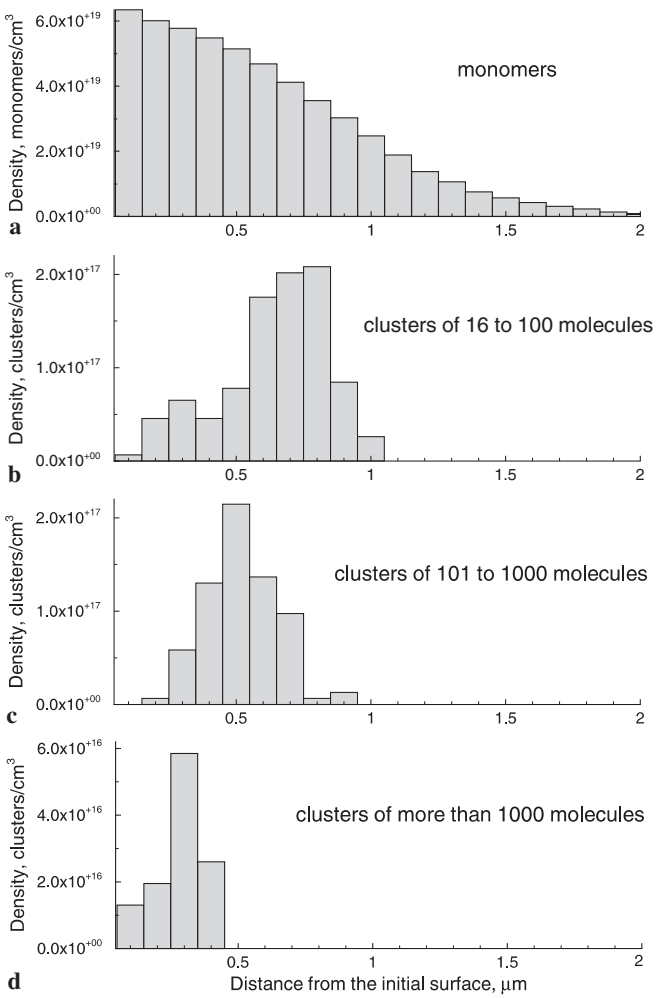

FIGURE 8 Number density of clusters of different sizes in the ablation plume as a funtion of the distance from the initial surface. The data is shown for 1 ns after irradiation with 150 ps laser pulse at a fluence of 61 J/m^2

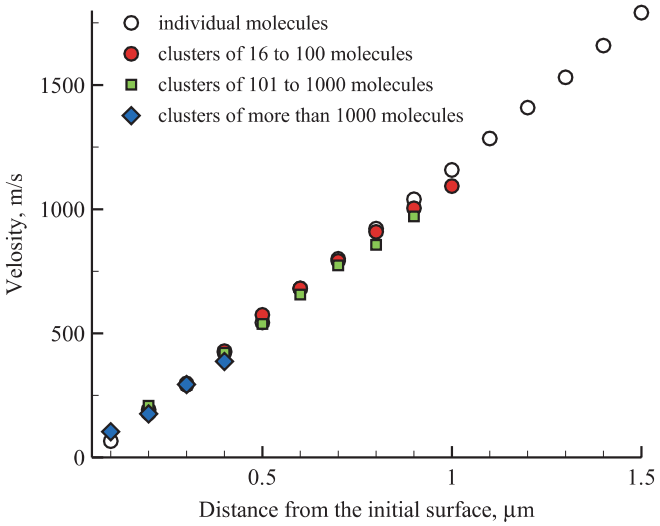

FIGURE 9 Flow velocity in the direction normal to the surface for the different components of the ablation plume as a function of the distance from the initial surface. The data is shown for 1 ns after irradiation with 150 ps laser pulse at a fluence of 61 J/m^2

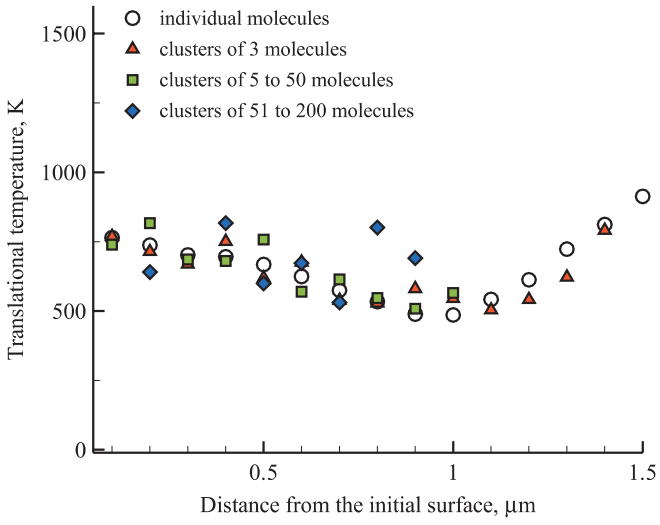

FIGURE 10 Translational temperature for monomers and clusters of different sizes in the ablation plume as a function of the distance from the initial surface. The translational temperature is calculated from the radial (parallel to the surface) velocity components of the ejected molecules or clusters. The data is shown for 1 ns after irradiation with 150 ps laser pulse at a fluence of 61 J/m^2

be related to the entrainment of large biomolecules into the plume of smaller matrix molecules in MALDI that has been observed experimentally [57] and in MD simulations [42, 44].

The spread in the radial velocities at a given distance from the surface can be described by a local translational temperature. The radial velocity components of molecules and clusters in the plume do not contain a contribution from the forwarded flow of the plume in the direction normal to the surface and thus can be associated with the thermal motion in the plume. As found in earlier simulations [32, 43, 44], the radial velocity distributions of ejected molecules fit well to a Maxwell–Boltzmann distribution, verifying that the spread of the radial velocities is associated with the thermal motion. The plot of the translational temperature of monomers and clusters of different sizes, Fig. 10, suggests that the same local translational temperature can be used to describe the spread of the radial velocities of the ejected molecules, small and medium-size clusters in the dense part of the plume. The effect of the local thermal equilibration of different plume components can be related to the earlier results of MD simulations of MALDI, when the radial velocity distributions for both matrix molecules and analyte molecules of different masses were found to fit well to a Maxwell–Boltzmann distribution with the same temperature [44]. The radial velocities of larger clusters are found to be significantly higher as compared to the thermal velocities. In particular, an average translational temperature calculated from the radial velocity component of clusters larger than 1000 molecules (there are 18 such clusters in this simulation) is found to be as high as 3080 K. Apparently, the collisions with the surrounding smaller species in the plume are not sufficient for thermal equilibration of the radial velocities of the largest clusters. Rather, these velocities reflect the dynamics of the active hydrodynamic motion of the liquid material during the ablation plume formation.

A significant variation of the translational temperature with distance from the irradiated surface, observed in Fig. 10, indicates that the fast cooling of the ejected material proceeds non-uniformly within the plume. Explosive cooling, when the thermal energy is transformed to the potential energy of disintegration of the overheated material and to the kinetic energy of the plume expansion, proceeds more efficiently in the top part of the plume and leads to the decrease of the temperature in the flow direction. At a certain distance from the surface, the translational temperature of monomers and small clusters reaches its minimum and starts to increase. This temperature increase can be attributed to the lack of equilibration in the front part of the expanding plume, where densities of ejected species are too small.

The internal energy/temperature of the ejected clusters is an important characteristic that defines the kinetics of evaporation/condensation processes and the result of cluster–cluster collision events during the long-term plume development. Figure 11 shows the internal temperature of clusters of different sizes, where the internal temperature of a cluster is defined from the kinetic energy of the translational molecular motion in the cluster center of mass frame of reference. The translational and vibrational degrees of freedom of molecules that belong to the same cluster are in equilibrium and the kinetic energy associated with these degrees of freedom can be described by the same internal temperature. Despite the large scattering of the data points for individual clusters, the overall tendency is clear – larger clusters in the plume have on the average substantially higher internal temperatures as compared to the smaller clusters. The internal temperature of the large clusters is also substantially higher than the translational (radial) temperature of the surrounding gas-phase molecules, 670 K in this simulation. The observed dependence of the internal temperature from the cluster size may seem to be counter-intuitive at first sight – larger clusters tend to originate from the regions deeper under the irradiated surface, where the energy density deposited by the laser pulse and the degree of the overheating are smaller. The lower temperature of the smaller clusters can be attributed, however, to a more vigorous phase explosion (a larger fraction of the gas-phase molecules

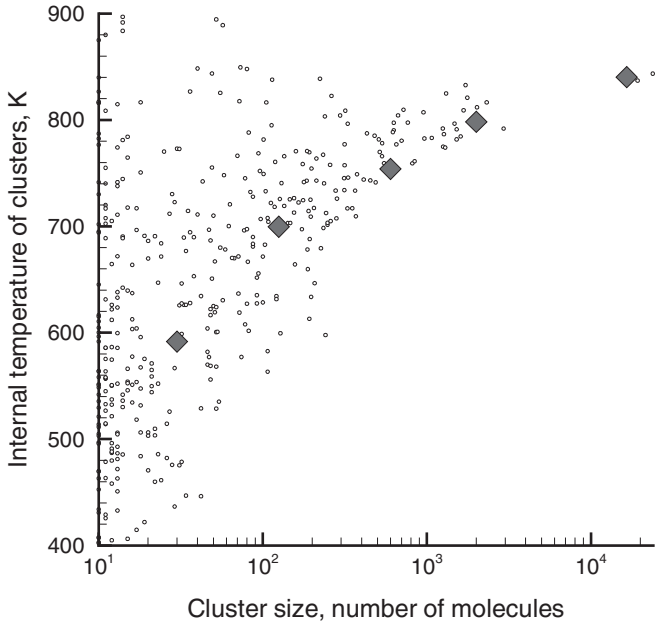

FIGURE 11 Internal temperature of clusters of different sizes (*small circles*). The internal temperature of a cluster is defined from the kinetic energy of the translational molecular motion calculated in the cluster center of mass frame of reference. Five *large diamonds* show the average temperatures of clusters that belong to the following ranges of sizes: from 10 to 50, from 50 to 200, from 200 to 1000, from 1000 to 3000, and from 3000 to 30000 molecules. The data is shown for 1 ns after irradiation with 150 ps laser pulse at a fluence of 61 J/m^2

is released due to a higher degree of overheating) and a fast expansion of the upper part of the plume. The vigorous phase explosion and the fast expansion of the plume provide a more efficient cooling as compared to a slower cooling of the larger clusters due to the evaporation. The same effect is responsible for the decrease of the translational temperature of the plume with distance from the irradiated surface, discussed above.

3.3 *The effect of the stress confinement*

The results of MD simulations suggest that in addition to the amount of energy supplied by the laser pulse and to the distribution of the energy within the sample, the rate of the energy deposition can be an important factor affecting the parameters of the ejected plume [32, 37]. In particular, it has been demonstrated that in the regime of stress confinement, when the laser pulse duration becomes shorter than the time of mechanical equilibration of the absorbing volume, a high thermoelastic pressure can result from the fast energy deposition and photomechanical effects start to play an important role in material ejection.

The difference between the character of material ejection in the regimes of thermal and stress confinement can be illustrated by comparison between the simulation discussed above (thermal confinement) and the one performed using the same laser fluence of 61 J/m^2, the same laser penetration depth of 50 nm, but ten times shorter laser pulse duration of 15 ps (stress confinement). A visual inspection of the snapshots from the simulations, Figs. 1 and 12, and a quantitative analysis of the ablation yields reveal both similarities and differences between the character of laser ablation in the thermal and stress confinement regimes. Although the decomposition of the overheated material proceeds in both cases through the formation of a transient structure of interconnected liquid regions, the decomposition is much faster in the stress confinement regime. Larger and more numerous clusters are ejected in the simulation with a 15-ps pulse as compared to

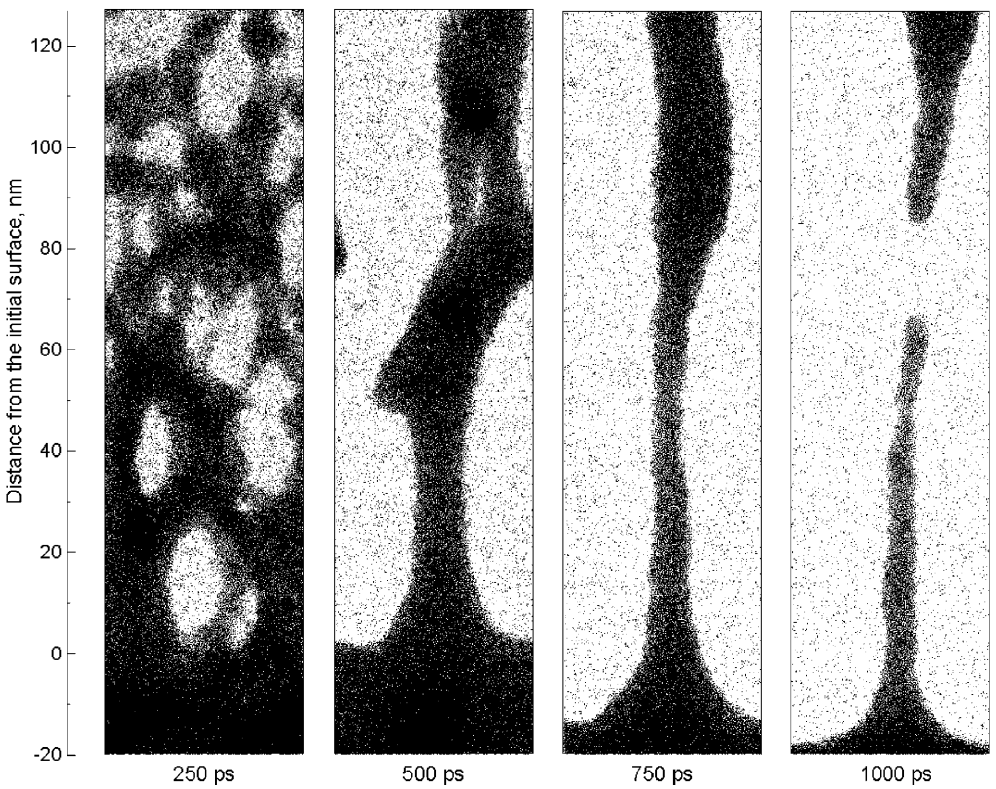

FIGURE 12 Snapshots from the simulation of laser ablation in the regime of stress confinement. The laser pulse duration is 15 ps and fluence is 61 J/m^2 (2.1 times the ablation threshold fluence)

a 150-ps pulse. The total amount of ejected material is ∼ 18% larger in the simulation with a 15-ps pulse, but the number of gas-phase molecules is ∼ 25% larger in the simulation with a 150-ps pulse. A more active, strongly forwarded hydrodynamic motion observed in the regime of stress confinement at 750–1000 ps, leads to the ejection of larger droplets. The hydrodynamic motion also results in the formation of large transient liquid bumps or asperities, such as the one at the snapshot taken at 1000 ps in Fig. 12. Evaporation and thermal conduction to the bulk of the target can lead to solidification of the asperities. These processes could be responsible for the formation of hydrodynamic patterns/asperities observed experimentally for metal targets, where thermal conduction is sufficient to provide fast cooling and freezing of the transient liquid surface features [16, 22, 23]. Note that the ejection of large droplets due to the hydrodynamic effects occurring on the scale of the whole laser spot cannot be investigated by the MD simulation technique and is beyond the scope of the present paper. Continuum computational approaches based on the solution of Navier–Stokes equations can be used to address this mode of cluster ejection [58, 59].

At lower laser fluences the fraction of the clusters in the ejected plume is increasing and the maximum size of the ejected droplets becomes larger in both thermal and stress confinement regimes. For the same laser fluence, however, the sizes of the droplets are always larger and the droplets constitute a larger portion of the plume in the stress confinement regime as compared to the thermal confinement regime. At fluences close to the ablation threshold, most of the ejected material can be ejected as a few large clusters or even a single cluster. In particular, in the simulation performed at 40 J/m^2, Fig. 13, the largest droplet accounts for ∼ 65% of the total amount of ejected material. At even lower laser fluence, close to the ablation threshold, a layer of relatively intact material can be separated from the bulk and ejected under the stress confinement irradiation conditions [32, 37, 38]. The mechanisms leading to the ejection of large and relatively cold chunks of material have been investigated and attributed to the mechanical fracture or spallation caused by the relaxation of high thermoelastic pressure [32]. In this case material disintegration is localized within the spallation region, at a certain depth under the surface, and proceeds through nucleation, growth, and coalescence of voids/microcracks.

3.4 *Cluster-size distributions*

The abundance distributions of the ejected clusters are shown in Fig. 14 for two simulations discussed above and illustrated by Figs. 1 and 12. In the cluster distributions, plotted on a double-logarithmic scale, one can readily distinguish two distinct regions that correspond to the small, up to ∼ 15 molecules, and large clusters. The cluster-size distributions can be relatively well described by a power law $Y(N) \sim N^{-\tau}$ with exponents different for low- and high-mass clusters. The decay is much slower in the high-mass region of the distributions – the exponent τ is 2–3 times larger. A power law for the cluster-yield distribution has been predicted for the gas–liquid phase transition occurring at the critical point [60]

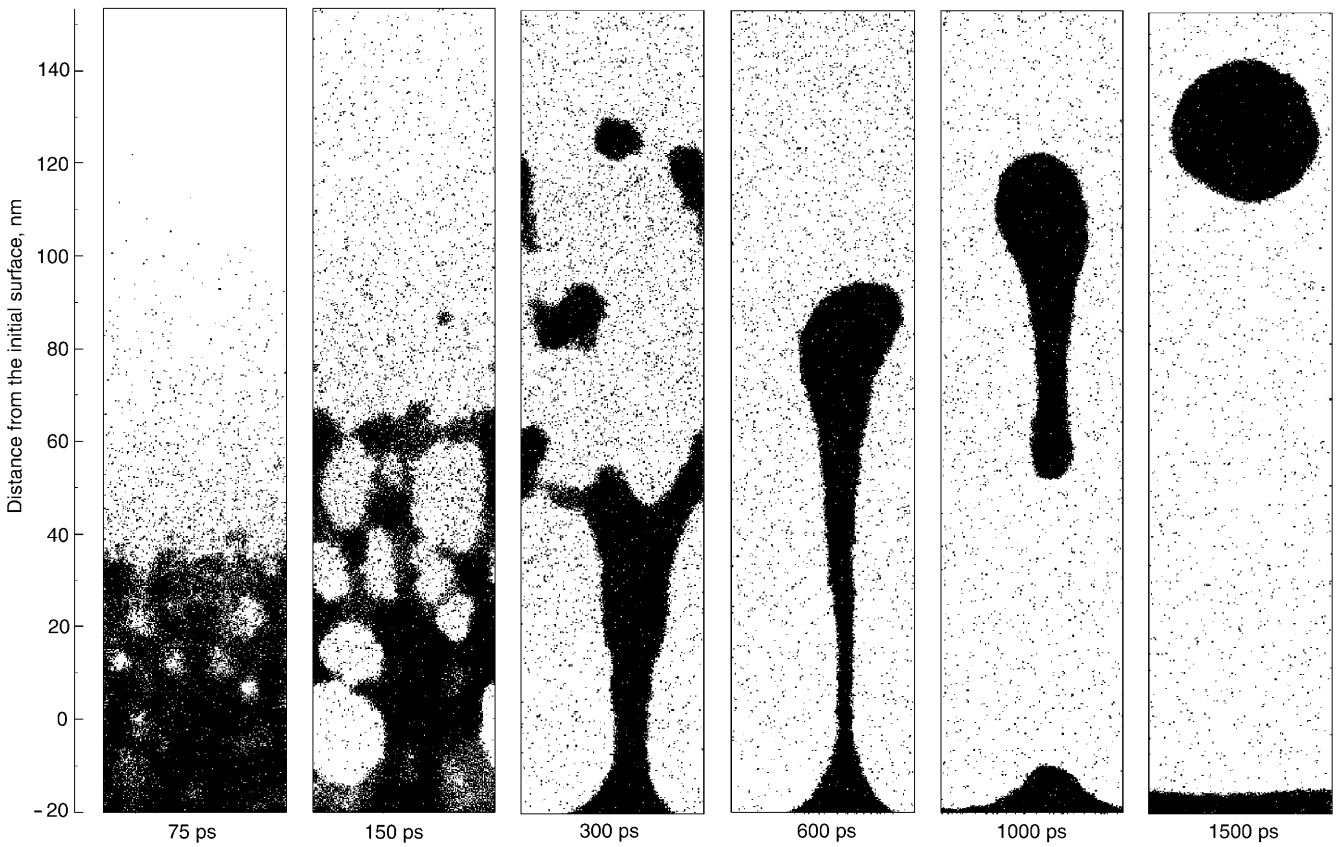

FIGURE 13 Snapshots from the simulation of laser ablation in the regime of stress confinement. The laser pulse duration is 15 ps and fluence is 40 J/m^2

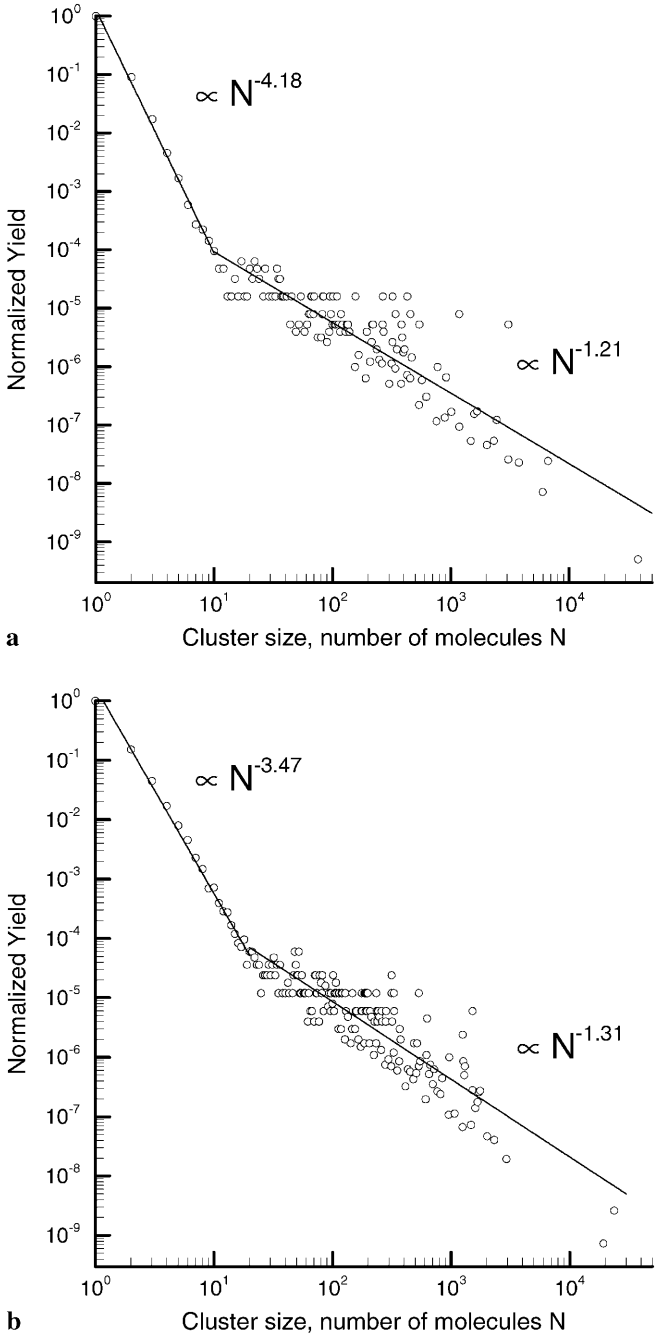

FIGURE 14 Cluster abundance distribution in the ablation plume at 1 ns after irradiation with **a** 15 ps and **b** 150 laser pulses at laser fluence of 61 J/m^2

and for self-similar fragmentation processes [61]. It has also been commonly observed in sputtering experiments [62, 63] and molecular dynamics simulations [63–66]. The complex character of the laser ablation process, however, makes it difficult to establish a direct link between any of the existing theoretical models and the results of the present simulations. Therefore, the fits to the power law are only used in this work to provide a quantitative description of the cluster-size distributions. Qualitatively, the existence of the two, low- and high-mass, regions in the cluster-abundance distributions can be related to the processes leading to the ablation plume formation, discussed above. The monomers and small clusters are released in the explosive decomposition of the overheated material into the liquid and vapor, whereas the larger clusters appear as a result of decomposition and coarsening of the transient liquid structure of interconnected liquid regions.

The existence of the two regions in the cluster-abundance distributions has been consistently observed in all simulations performed to date for both thermal and stress confinement at laser fluences sufficiently high to produce a statistically significant number of large clusters. The dependence of the exponent in the power-law fit of the abundance distribution on irradiation parameters is the subject of current investigation. Preliminary results indicate that in the low-mass region the exponent increases with fluence (absolute value of $-\tau$ decreases) and, for a given fluence, is always higher in the thermal confinement regime. In the high-mass regime the exponent decreases with fluence and, for a given fluence, is higher in the stress confinement regime. The observed range of the exponent is from -5 to -3.2 for the low-mass region and from -1.3 to -0.9 for the high-mass region.

4 Summary

The results of large-scale MD simulations of laser ablation provide insights into complex processes occurring at the early stages of the ablation plume development and their relation to the parameters of the ejected clusters. The cluster composition of the ablation plume is found to have a strong dependence on the irradiation conditions and is defined by the interplay of a number of processes during the ablation plume evolution.

At sufficiently high laser fluences, the dominant mechanism responsible for material ejection is the phase explosion of the material overheated up to the limit of its thermodynamic stability. The phase explosion leads to the rapid decomposition of the surface region of the target into a mixture of liquid droplets, gas-phase molecules, and small molecular clusters. This decomposition proceeds through the formation of a foamy transient structure of interconnected liquid regions. There is a strong dependence of the character of material decomposition on the depth of origin of the ejected material. Overheating becomes weaker with increasing depth, the fraction of the liquid phase increases and large droplets are formed in the tail of the plume.

The effect of segregation of the clusters of different sizes in the expanding plume is observed in the simulations. There is a relatively small number of small and medium clusters in the region adjacent to the surface, where large clusters are being formed. Medium-size clusters dominate in the middle of the plume and only small clusters and monomers are observed near the front of the expanding plume.

Despite being ejected from deeper under the surface, where the absorbed energy density is smaller, the larger clusters in the plume have substantially higher internal temperatures as compared to the smaller clusters. The lower temperature of the smaller clusters can be attributed to a more efficient cooling due to phase explosion and a fast expansion of the upper part of the plume as compared to a slower cooling of the larger clusters, dominated by evaporation.

In simulations performed with shorter laser pulses, in the regime of stress confinement, a contribution of the laser-

induced thermoelastic stresses leads to a more active, strongly forwarded hydrodynamic motion in the vicinity of the melted surface. This in turn leads to the ejection of larger and more numerous droplets as compared to the regime of thermal confinement. At low laser fluences, close to the ablation threshold, relaxation of high thermoelastic pressure in the regime of stress confinement can cause the mechanical fracture/spallation and ejection of large and cold chunks of relatively intact material.

In the cluster-abundance distribution one can distinguish two distinct regions that correspond to small, up to ~ 15 molecules, and large clusters. The cluster-size distributions can be relatively well described by a power law $Y(N) \sim N^{-\tau}$ with exponents different for the small and large clusters. The decay is much slower in the high-mass region of the distribution.

ACKNOWLEDGEMENTS Financial support of this work was provided by the University of Virginia through the new faculty start-up funds and the Air Force Office of Scientific Research through the Medical Free Electron Laser Program. Partial computational support was provided by the National Partnership for Advanced Computational Infrastructure (NPACI) program. The author would like to thank B.J. Garrison and R.E. Johnson for insightful and stimulating discussions.

REFERENCES

1 D. Bäuerle: *Laser Processing and Chemistry* (Springer, Berlin, Heidelberg 2000)
2 D.B. Chrisey, G.K. Hubler (eds.): *Pulsed Laser Deposition of Thin Films* (Wiley-Interscience, New York 1994)
3 M.H. Niemz: *Laser–tissue Interactions: Fundamentals and Applications* (Springer, Berlin, Heidelberg 1996)
4 F. Hillenkamp, M. Karas, R.C. Beavis, B.T. Chait: Anal. Chem. **63**, 1193A (1991)
5 F. Hillenkamp, M. Karas: Int. J. Mass Spectrom. **200**, 71 (2000)
6 J. Heitz, J.T. Dickinson: Appl. Phys. A **68**, 515 (1999)
7 P. Ayyub, R. Chandra, P. Taneja, A.K. Sharma, R. Pinto: Appl. Phys. A **73**, 67 (2001)
8 E. Borsella, S. Botti, R. Giorgi, S. Martelli, S. Turtù, G. Zappa: Appl. Phys. Lett. **63**, 1345 (1993)
9 M. Karas, U. Bahr, F. Hillenkamp: Int. J. Mass Spectrom. Ion Proc. **92**, 231 (1989)
10 V. Karbach, R. Knochenmuss: Rapid Commun. Mass Spectrom. **12**, 968 (1998)
11 M. Karas, M. Glückmann, J. Schäfer: J. Mass Spectrom. **35**, 1 (2000)
12 I. Fournier, A. Brunot, J.C. Tabet, G. Bolbach: Int. J. Mass Spectrom. **213**, 203 (2002)
13 M. Handschuh, S. Nettesheim, R. Zenobi: Appl. Surf. Sci. **137**, 125 (1999)
14 B.N. Kozlov, B.A. Mamyrin: Tech. Phys. **44**, 1073 (1999)
15 R.L. Webb, J.T. Dickinson, G.J. Exarhos: Appl. Spectrosc. **51**, 707 (1997)
16 A.B. Brailovsky, S.V. Gaponov, V.I. Luchin: Appl. Phys. A **61**, 81 (1995)
17 H. Mizuseki, Y. Jin, Y. Kawazoe, L.T. Wille: Appl. Phys. A **73**, 731 (2001)
18 G. Callies, H. Schittenhelm, P. Berger, H. Hügel: Appl. Surf. Sci. **127–129**, 134 (1998)
19 M. Kuwata, B. Luk'yanchuk, T. Yabe: Proc. SPIE **4065**, 441 (2000)
20 S.M. Hankin, P. John: J. Phys. Chem. B **103**, 4566 (1999)
21 K.H. Song, X. Xu: Appl. Surf. Sci. **127–129**, 111 (1998)
22 T.D. Bennett, C.P. Grigoropoulos, D.J. Krajnovich: J. Appl. Phys. **77**, 849 (1995)
23 X. Zhang, S.S. Chu, J.R. Ho, C.P. Grigoropoulos: Appl. Phys. A **64**, 545 (1997)
24 J.H. Yoo, S.H. Jeong, X.L. Mao, R. Greif, R.E. Russo: Appl. Phys. Lett. **76**, 783 (2000)
25 J.H. Yoo, S.H. Jeong, R. Greif, R.E. Russo: J. Appl. Phys. **88**, 1638 (2000)
26 A. Okano, K. Takayanagi: Appl. Surf. Sci. **127–129**, 362 (1998)
27 M.M. Martynyuk: Sov. Phys. Tech. Phys. **21**, 430 (1976)
28 A. Miotello, R. Kelly: Appl. Phys. A **69**, S67 (1999)
29 R. Kelly, A. Miotello: J. Appl. Phys. **87**, 3177 (2000)
30 N.M. Bulgakova, A.V. Bulgakov: Appl. Phys. A **73**, 199 (2001)
31 L.V. Zhigilei, B.J. Garrison: Appl. Phys. Lett. **74**, 1341 (1999)
32 L.V. Zhigilei, B.J. Garrison: J. Appl. Phys. **88**, 1281 (2000)
33 R. Kelly, J.E. Rothenberg: Nucl. Instrum. Methods B **7–8**, 755 (1985)
34 D.E. Hare, J. Franken, D.D. Dlott: J. Appl. Phys. **77**, 5950 (1995)
35 G. Paltauf, H. Schmidt-Kloiber: Appl. Phys. A **62**, 303 (1996)
36 L.V. Zhigilei, P.B.S. Kodali, B.J. Garrison: Chem. Phys. Lett. **276**, 269 (1997)
37 L.V. Zhigilei, B.J. Garrison: Appl. Phys. A **69**, S75 (1999)
38 A.G. Zhidkov, L.V. Zhigilei, A. Sasaki, T. Tajima: Appl. Phys. A **73**, 741 (2001)
39 I. Itzkan, D. Albagli, M.L. Dark, L.T. Perelman, C. von Rosenberg, M.S. Feld: Proc. Natl. Acad. Sci. USA **92**, 1960 (1995)
40 A.A. Oraevsky, S.L. Jacques, F.K. Tittel: J. Appl. Phys. **78**, 1281 (1995)
41 R. Cramer, R.F. Haglund Jr., F. Hillenkamp: Int. J. Mass Spectrom. Ion Proc. **169–170**, 51 (1997)
42 L.V. Zhigilei, P.B.S. Kodali, B.J. Garrison: J. Phys. Chem. B **101**, 2028 (1997); J. Phys. Chem. B **102**, 2845 (1998)
43 L.V. Zhigilei, B.J. Garrison: Appl. Phys. Lett. **71**, 551 (1997)
44 L.V. Zhigilei, B.J. Garrison: Rapid Commun. Mass Spectrom. **12**, 1273 (1998)
45 L.V. Zhigilei, B.J. Garrison: In: *Multiscale Modelling of Materials*, ed. by T. Diaz de la Rubia, T. Kaxiras, V. Bulatov, N.M. Ghoniem, R. Phillips (Mater. Res. Soc. Symp. Proc. **538**) (Materials Research Society, Warrendale, 1999) p. 491
46 H. Häkkinen, U. Landman: Phys. Rev. Lett. **71**, 1023 (1993)
47 C. Schäfer, H.M. Urbassek, L.V. Zhigilei: Phys. Rev. B **66**, 115404 (2002)
48 L.V. Zhigilei, A. Dongare: Comp. Model. Eng. Sci. **3**, 539 (2002)
49 D.S. Ivanov, L.V. Zhigilei: in preparation
50 P. Lorazo, L.J. Lewis, M. Meunier: Appl. Surf. Sci. **168**, 276 (2000)
51 K. Dreisewerd, M. Schürenberg, M. Karas, F. Hillenkamp: Int. J. Mass Spectrom. Ion Proc. **154**, 171 (1996)
52 L.V. Zhigilei: In: *Advances in Materials Theory and Modeling – Bridging Over Multiple-length and Time Scales*, ed. by V.V. Bulatov, F. Cleri, L. Colombo, L.J. Lewis, N. Mousseau (Mater. Res. Soc. Symp. Proc. **677**) (Materials Research Society, Warrendale, 2001) AA2.1.1
53 L. Ming, N. Marković, M. Svanberg, J.B.C. Pettersson: J. Phys. Chem. A **101**, 4011 (1997)
54 S. Murad, C.K. Law: Mol. Phys. **96**, 81 (1999)
55 M.I. Zeifman, B.J. Garrison, L.V. Zhigilei: in *Modeling and Numerical Simulation of Materials Behavior and Evolution*, ed. by V. Tikare, E.A. Olevsky, A. Zavaliangos (Mat. Res. Soc. Symp. Proc. **731**) (Materials Research Society, Warrendale, 2002) W3.8.1
56 M.I. Zeifman, B.J. Garrison, L.V. Zhigilei: J. Appl. Phys. **92**, 2181 (2002)
57 A.A. Puretzky, D.B. Geohegan, G.B. Hurst, M.V. Buchanan, B.S. Luk'yanchuk: Phys. Rev. Lett. **83**, 444 (1999)
58 N. Seifert, G. Betz: Appl. Surf. Sci. **133**, 189 (1998)
59 M. Jakas: private communication (2001)
60 H.M. Urbassek: Nucl. Instrum. Methods Phys. Res. B **31**, 541 (1988)
61 A. Bershadskii: Eur. Phys. J. B **14**, 323 (2000)
62 A.V. Hamza, T. Schenkel, A.V. Barnes: Eur. Phys. J. D **6**, 83 (1999)
63 T.J. Colla, H.M. Urbassek, A. Wucher, C. Staudt, R. Heinrich, B.J. Garrison, C. Dandachi, G. Betz: Nucl. Instrum. Methods Phys. Res. B **143**, 284 (1998)
64 A. Wucher, B.J. Garrison: J. Chem. Phys. **105**, 5999 (1996)
65 T. Muramoto, M. Okai, Y. Yamashita, K. Yorizane, Y. Yamamura: Nucl. Instrum. Methods Phys. Res. B **180**, 222 (2001)
66 T.J. Colla, H.M. Urbassek: Comput. Mater. Sci. **6**, 7 (1996)